



OPEN ACCESS

EDITED BY

Andrea Scagliarini,
National Research Council (CNR), Italy

REVIEWED BY

Zeeshan Asghar,
Prince Sultan University, Saudi Arabia
Prateek Kattimani,
Davangere University, India

*CORRESPONDENCE

Rania Saadeh,
✉ r.saadeh@bau.edu.jo

†PRESENT ADDRESS

Ayodeji Felix Isarinade,
Department of Geosciences, Baylor
University, Waco, TX, United States

RECEIVED 06 November 2025

REVISED 24 December 2025

ACCEPTED 13 January 2026

PUBLISHED 12 February 2026

CITATION

Saadeh R, Alrebdi S, Obalalu AM, Isarinade AF and Khan U (2026) Numerical simulations using finite-element scheme for the optimization of micropolar tri-hybrid nanofluids with periodic gravitational disturbance and heat source/sink effects. *Front. Phys.* 14:1740818. doi: 10.3389/fphy.2026.1740818

COPYRIGHT

© 2026 Saadeh, Alrebdi, Obalalu, Isarinade and Khan. This is an open-access article distributed under the terms of the [Creative Commons Attribution License \(CC BY\)](https://creativecommons.org/licenses/by/4.0/). The use, distribution or reproduction in other forums is permitted, provided the original author(s) and the copyright owner(s) are credited and that the original publication in this journal is cited, in accordance with accepted academic practice. No use, distribution or reproduction is permitted which does not comply with these terms.

Numerical simulations using finite-element scheme for the optimization of micropolar tri-hybrid nanofluids with periodic gravitational disturbance and heat source/sink effects

Rania Saadeh^{1*}, Suad Alrebdi², A. M. Obalalu³,
Ayodeji Felix Isarinade^{4†} and Umair Khan^{5,6}

¹Department of Applied Science, Ajloun College, Al-Balqa Applied University, Ajloun, Jordan,

²Department of Entrepreneurship, Entrepreneurship Institute, King Saud University, Riyadh, Saudi Arabia, ³Department of Mathematics and Statistics, Kwara State University, Malete, Nigeria,

⁴Department of Mathematics and Data Science, Wigwe University, Isiokpo, Rivers State, Nigeria,

⁵Department of Mathematics, Saveetha School of Engineering, Saveetha Institute of Medical and Technical Sciences, Saveetha University, Chennai, Tamil Nadu, India, ⁶Department of Mathematics, Faculty of Science, Sakarya University, Sakarya, Türkiye

Advancing heat transfer mechanisms in gravitationally varying environments is crucial for improving engineering applications in aerospace engineering, astrophysics, spacecraft, and satellites. Motivated by these applications, this study examines the influence of periodic variations in gravitational acceleration and externally applied magnetic fields on heat and momentum transfer over an inclined stretching sheet situated in an upper-atmosphere or microgravity regime. The thermophysical properties of glycerine, carbon nanotubes (CNTs), gold (Au), and aluminum oxide (Al₂O₃) are incorporated to evaluate their contributions to enhancing thermal conductivity and heat transport performance. The transformed governing equations are numerically solved using the finite element method (FEM), with simulations executed in Wolfram Mathematica to assess the impact of key physical parameters. The results indicate that hybrid and ternary hybrid nanofluids substantially outperform mono nanofluids. Specifically, the ternary hybrid nanofluid yields up to a 31.6% increase in temperature distribution and a 27.4% rise in velocity magnitude relative to the base nanofluid. An increase in the micropolar material parameter enhances fluid motion, producing an 18.2% increase in velocity, while increasing the Hartmann number reduces the velocity by approximately 22.9%, confirming the expected magnetic damping effect. Additionally, both the skin-friction coefficient and the Nusselt number increase with higher gravity modulation amplitudes, showing up to a 24.7% rise in shear stress and a 29.3% improvement in heat transfer rate. Overall, the findings demonstrate the superior heat transport capability of ternary hybrid nanofluids under fluctuating gravity conditions, highlighting their potential

for advanced thermal management in space and microgravity engineering applications.

KEYWORDS

finite element method (FEM), g-jitter (periodic microgravity), inclined stretching surface, magnetohydrodynamics (MHD), micropolar ternary hybrid nanofluids

1 Introduction

Ternary hybrid nanofluids are an advanced kind of thermal transport fluids containing three varieties of nanoparticle dispersed in a base fluid. THNFs are fluids that comprise three different kinds of nanoparticles. Each nanoparticle has its own unique thermal, chemical, and physical advantages. By mixing all three types into one base fluid, researchers aim to combine the strengths of each particle [1]. THNFs have a better thermal and rheological characteristic due to the combination of thermal advantages of both NPs, as well as increased surface area, thermal stability, and thermal conductivity of the thermal nanoparticles [2]. This high performance leads to them being extremely useful in use in energy systems, microelectronics cooling, solar collectors, and biomedical device. The improvement of THNFs is mainly driven via the necessity to increase the energy efficiency of cooling and heating systems. In many advanced applications, traditional thermal transport fluids are often insufficient to meet the demanding performance requirements. Consequently, innovative fluid formulations are vital to attain enhanced temperature stabilization and reliability in high-performance environments [3]. The ternary hybrid nanofluids are very important since they could be used in enhancing significantly applications that are based on effective heat dissipation and heat control. Due to their improved properties, they can be used as promising candidates in applicability on both electronics cooling, automotive thermal systems, solar collectors and also heat exchangers where control of high heat fluxes are important. These fluids hold the potential in solving problems in the emerging fields like microchannel cooling, concentrated photovoltaic systems, and advanced manufacturing processes through the means of optimizing performance, which is minimized by the usage of energy. Besides, the study of ternary hybrid nanofluids helps the understanding of multiphase flow, the interaction of nanomaterials, and the stability of fluids which enhances innovation in the field of material science and thermal engineering [4]. [5] examine the thermal performance of THNFs and binary nanofluid flows under the effect of thermal conductivity, heterogeneous catalytic reaction, heat source/sink, radiation, and the suction/injection. They study the thermal transport and the enhancement of autocatalysis in THNFs with the help of the Hamilton-Crosser model and considering a Riga wedge. [6] explore the flow and heat transfer of copper nanoparticles titanium dioxide nanoparticles (TiO₂ NPs), silver nanoparticles (Ag NPs) nanoparticles across an exponentially contracting/extending surface, which can be used in polymer processing, fibre manufacturing and power generation. The model considers modified Darcy law where inertial effects in a porous medium are taken into consideration, radiative heat flux, and variable heat sources, and suction as well as magnetic fields. [7] considered the effects of a heat source/sink and thermal radiation to study the bioconvection of an Al₂O₃-Graphene-CNT/water ternary

hybrid nanofluid containing motile microorganisms between two infinitely parallel spinning disks in a porous medium.

Gravity modulation refers to the process of altering or controlling gravitational effects, either naturally or artificially, within a localized region or over a broader area. The study of gravity modulation occurs at the connection of standard physics, general relativity, and speculative high-tech applications, reflecting both theories and projected developments [8]. Traditionally, gravity has been one of the fundamental forces of nature, which in Newtonian mechanics is defined as a universal attraction between masses and further advanced by Einstein general theory of relativity which defines gravity as the curvature of spacetime by mass and energy [9]. Gravity modulation is a research topic with great theoretical and applied physics significance. In case this is overcome there will be a revolution in transportation, energy and space exploration. Such ideas might have a realistic implementation via the creation of all-new propulsion systems, making space travel not only speedy but also very efficient, even without the traditional notion of fuel consumption. Minor taming of the local gravitational fields on Earth could provide a breakthrough in construction works, mining, and handling of materials, where the weight of objects is always a crucial limitation. Moreover, advances in this field could lead to a better understanding of unification theories, quantum gravity and the underlying structure on spacetime, which will have the potential of revolutionary applications far beyond their technological purpose [10]. [11] investigated the stability of a porous medium subjected to a vertically inclined magnetic field, taking into account the modulation of internal heat, chemical reactions, and gravity. Their findings indicate that gravity modulation influences the heat and mass transfer that are manifested in the Nusselt and Sherwood values. [12] analyzed the problem of triple-diffusive convection (TDC) of two solutes and an internal heat source between two infinite flat plates under gravity modulation. They discuss the influence of a gravity modulation in cases pertinent to the space vehicles and geothermal systems in connection with the transportation of heat and mass.

Magnetohydrodynamics (MHD) is the study of the dynamics of electrically conducting fluids in a magnetic field. It joins the elements of fluid mechanics and electromagnetism to explain the interaction between magnetic fields and plasmas, liquid metals or saltwater [13]. MHD governing equations are obtained by coupling Navier-Stokes with Maxwell equations to formulate a system that can describe the complicated interactions between flow velocity, pressure, density and flow electric current and magnetic fields. A broad variety of phenomena, including the structure of astrophysical jets and the dynamics of stellar interiors and stability of fusion plasmas, are illuminated by this theoretical basis. The importance of magnetohydrodynamics is its ability to facilitate the comprehension of the systems in which fluid at motion and magnetic fields are interconnected [14]. It makes possible the invention of

technologies to produce and trap high-temperature plasmas in fusion reactors, which is to supply a source of energy at sustainable levels. The behaviour of solar flares, planetary magnetospheres and galactic magnetic fields also play an important role in comprehending the solar systems, which is a key in interpretations using MHD principles. Magnetohydrodynamics has numerous industrial applications like electromagnetic casting of metal, MHD generator and nuclear reactor cooling systems. In regards of this, the recent work of [15] examine the magnetohydrodynamics micropolar fluid flow and thermal transport across curved surfaces with thermal radiation effects. [16] examine the unsteady magneto hydrodynamics and influence of the Hall current in the incompressible Jeffrey fluid flow with a vertical plate having heat absorption and chemical reaction.

A heat source or sink is the system or material that transports or receives thermal energy to allow the transmission of heat in an actual surrounding. The idea of heat sources and sinks is central to thermodynamics where it is applied to describe energy as exchanged by a system and its surroundings. Physically, heat sources supply thermal energy that may be used to cause phase transitions, reactions or mechanical activities and heat sinks absorb this energy and are often used to control or stabilize the temperature. These concepts are entrenched in the infrastructure of engines, refrigeration cycles, climatic models and other natural and constructed designs [17]. The presence of heat sources and sinks on Earth from the warming effect of the sun to the cooling effect of radiators helps maintain the thermal balance essential for both technological operations and natural processes. Heat sources and sinks should be well understood and their management essential to subjects such as energy systems as well as environmental science. They play a leading part in the production of effective power generation, heating, ventilation, and air-conditioning systems and thermal control of electronics and equipment. The principle of heat transfer where the artificial sinks and sources are controlled in space exploration will assure the survival of instruments and crews in extreme conditions. Therefore, the heat sources and sinks in climate change are essential for the prediction and mitigation of the effects of climate change in the planet. [18] discuss the thermal transfer performance of heat source/sink on the nonlinear radiating plate that is vertical. They apply non-dimensional analysis and solve the problem using the implicit finite difference method to determine the effect of the main parameters on velocity, temperature, skin-friction and heat-mass transfer.

Thermal radiation is a type of heat transfer which occurs through electromagnetic radiations emitted by all bodies as result of their temperature. In contrast to conduction and convection, the thermal radiation requires no medium to take place, nor does it require presence of a medium when it happens in a vacuum. It is controlled by some basic laws like the Plancks law, Stefan Boltzmann law, and the Wien displacement law, which explains the intensity and spectral distribution of radiation in relation to temperature [19]. Radiative heat exchange has numerous significant applications in both natural and industrial systems, such as thermal climate management, combustion systems and space. Thermal radiation has played a significant function in quantum and relativistic physics, and investigations into blackbody radiation directly contributed to the development of quantum theory. Also, Thermal radiation plays an essential role in energy exchange and thermals management

in science and technology, which makes the study and control of such radiation very important. In engineering, thermal radiation is used to design insulating materials, radiators, and heat shields. In spacecraft, the thermal radiators are used to control the high heat in space technology in the form of a vacuum [20]. Infrared the image of radiations is known as thermal imaging and is used in surveillance, medical diagnosis and industrial monitoring. Moreover, thermal radiation is critical in atmospheric sciences where it is used in climate models in terms of predicting energy balance on Earth and greenhouse effect. Innovation in energy efficiency, materials science and remote sensing is still being fuelled by developments in controlling emissivity and absorptivity at different wavelengths. [21] inspect the 3-dimensional nonlinear thermal diffusion, thermal radiation, and nanofluid flow near a stretchable boundary, considering the Lorentz force within the microstructural framework by treating the flow as a boundary layer flow [22]. examine the thermal radiation and heat convection of the Casson fluid blood that is combined with nanoparticles of copper and Al_2O_3 with water based fluid.

The Micropolar fluid theory is a classical mechanics of fluids in which it takes into consideration of microstructure and intrinsic rotation of the fluid particles and it provides a more detailed description of fluids that have rigid or semi rigid microscopic components. Micropolar fluids illustrate the couple stresses and show the microrotation effects which are differ from the Newtonian fluids [23]. In 1960s, Eringen proposed this kind of fluid such fluids (including suspensions, liquid crystals, polymeric fluids and some biological fluids) in which the internal structure plays an important role in the fluid dynamics. This Micropolar fluid model is used to add other field quantities (microrotation vector, couple stress tensor. The study of Micropolar fluid model gives a better description of materials whose microstructural effects cannot be ignored. This can be directly related to the forecasting of blood flow behavior, lubricants with additives, colloidal suspensions and other complex fluids that can be found in biomedical engineering, material processing and industrial practice. Micropolar models prove to be important in the modelling of microfluid and nanotechnology where length scales are small and surface or microstructure effects become important towards the design of efficient systems and devices. [24] studied heat transfer viscoelastic-micropolar fluid behavior in the rotating flow of elastic fluids over a vertical isothermal cone, considering two-dimensional laminar flow and. They investigated the effects of various parameters on thermo-fluid properties using similarity variables, with the reduced boundary layer equations solved via the Keller Box method in MATLAB. The study found that an increase in the extended relaxation time leads to a thinner thermal boundary layer and enhances fluid transport. On IFDM simulation of Oldroyd 8-constant fluid flowing due to motile microorganisms were study by [25]. Surface roughness effects on the propelling mechanism of spermatozoa were study by [26]. Magnetohydrodynamic flow of Carreau Yasuda fluid inside a complex wavy passage formed by beating cilia were study by [27]. A numerical framework for modeling the dynamics of micro-organism movement on Carreau-Yasuda layer were study by [28]. An IFDM analysis of low Reynolds number flow generated in a complex wavy curved passage formed by artificial beating cilia were study by [29]. CVFEM simulation for Fe_3O_4 - H_2O nanofluid in an annulus between two triangular

enclosures subjected to magnetic field and thermal radiation were study by [30].

This study investigates the thermal and momentum behavior of micropolar nanofluids and hybrid nanofluids flowing over an extending inclined surface within an upper-space environment influenced by periodic microgravity and a transverse magnetic field. The flow is governed by mixed convection due to g-jitter effects, with a particular focus on comparing the heat and fluid transport characteristics of glycerine, carbon nanotubes (CNTs), gold (Au), and aluminum oxide (Al₂O₃). The governing boundary layer equations are reduced to a system of nonlinear ordinary differential equations using similarity transformations and are then numerically solved using the finite element method. A MATLAB-based simulation is implemented to evaluate the impact of key physical parameters such as the Hartmann number, micropolar parameter, gravity modulation amplitude, and heat source/sink on fluid velocity, temperature distribution, skin friction, and heat transfer rate. The aim and objective of this study is to develop a finite-element-based computational framework for analyzing the influence of periodic gravity modulation, magnetic fields, and micropolar material effects on the thermo-fluid dynamics of micropolar mono and hybrid nanofluids over an inclined stretching surface, with the goal of enhancing the understanding of heat and momentum transfer performance under upper-space microgravity conditions.

2 Governing laws associated with the model

- We consider the influence of microgravity on the flow behavior and thermal properties of non-Newtonian fluids over a stretching inclined plate with ambient temperature \check{T}_∞ , applied magnetic field B_0 , wall temperature \check{T}_w , and inclination angle γ as illustrated in Figure 1A.
- The plate stretches along the x -axis, and its surface normal lies along the y -axis. The plate velocity is linearly dependent on the spatial coordinate and is given by $\check{u}_w = bx$, where $b > 0$
- It is assumed that there is no slip between the base fluid and the suspended nanoparticles, and thermal equilibrium is maintained between phases.

The momentum balance incorporates the effect of an oscillating gravitational force, expressed as:

$$g^*(t) = [g_0 + ag_0 \cos(\pi\omega t)] \tag{1}$$

where g_0 represents the average gravitational acceleration, a is the amplitude of oscillation, ω is the frequency, and t denotes time. The gravitational force is considered to act along the upward direction, aligned with the unit vector k . Taking these assumptions into account, the governing equations for the problem namely, the continuity, momentum, micropolar and energy equations are [20]:

$$\frac{\partial \check{U}_1}{\partial x} + \frac{\partial \check{U}_2}{\partial y} = 0 \tag{2}$$

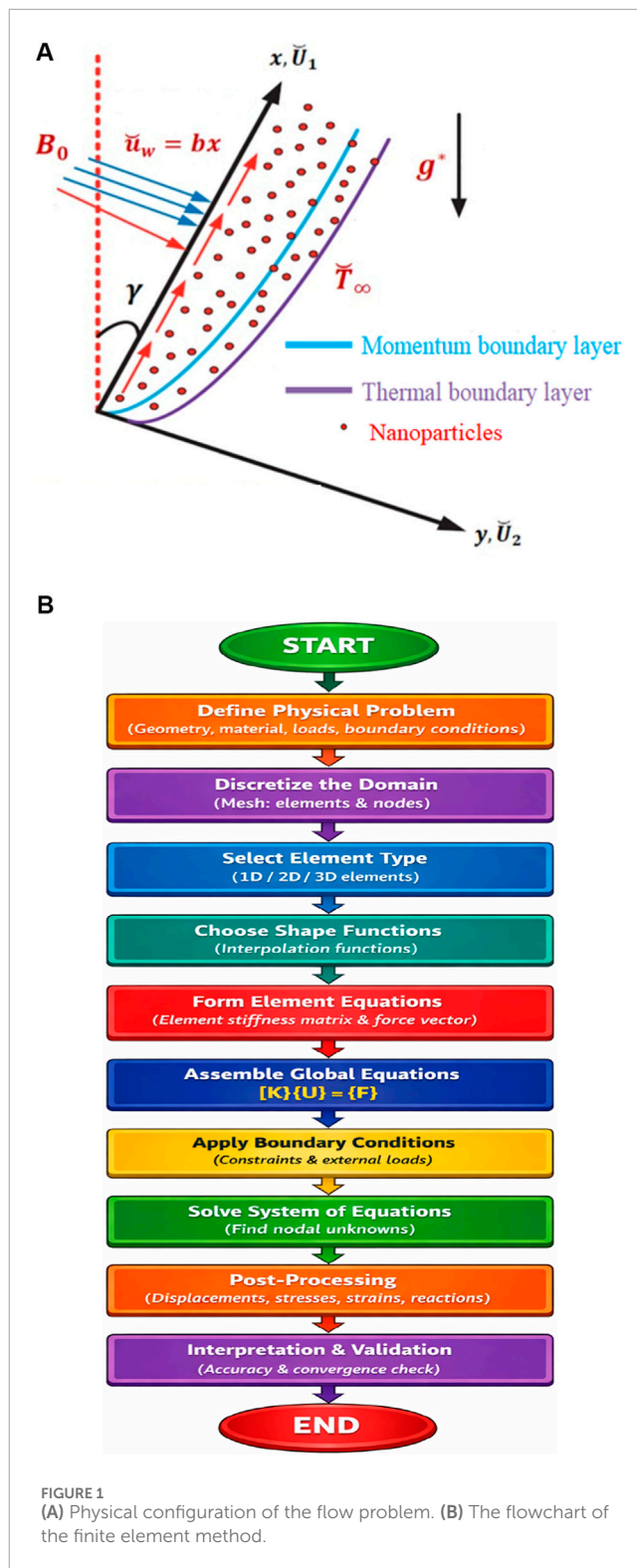


FIGURE 1 (A) Physical configuration of the flow problem. (B) The flowchart of the finite element method.

$$\begin{aligned} & \rho_{thnf} \left(\frac{\partial \check{U}_1}{\partial t} + \check{U}_1 \frac{\partial \check{U}_1}{\partial x} + \check{U}_2 \frac{\partial \check{U}_1}{\partial y} \right) \\ & = (\mu_{thnf} + \kappa) \frac{\partial^2 \check{U}_1}{\partial y^2} \\ & \quad - \sigma_{thnf} B_0^2 \check{U}_1 + \kappa \frac{\partial \check{N}}{\partial y} - \frac{\mu_{thnf}}{K_p} \check{U}_1 + g^*(t) ((\rho\beta)_{thnf}) (\check{T} - \check{T}_\infty) \cos \gamma \end{aligned} \tag{3}$$

TABLE 1 Symbol and description.

Symbol	Description	Symbol	Description
\check{U}_1, \check{U}_2	Velocity components in x and y directions	\check{T}	Temperature of the fluid
\check{N}	Angular (microrotation) velocity of the fluid	C_p	Specific heat capacity of the fluid
ρ_{thnf}	Density of the THN	Q_0	Internal heat generation or absorption
μ_{thnf}	Dynamic viscosity of THN	κ	Vortex/spin (microrotation) viscosity
σ_{thnf}	Electrical conductivity of the THN	$\tilde{\alpha}$	Thermal diffusivity
β	Thermal expansion coefficient	$\gamma^* = j(\mu_{thnf} + \frac{\kappa}{2})$	Fluid spin gradient viscosity
j	Microinertia density	$K = \frac{\kappa}{\mu_f}$	Dimensionless vortex viscosity parameter
σ^*, k^*	Stefan-Boltzmann constant, mean absorption coefficient		

$$\rho_{thnf} j \left(\frac{\partial \check{N}}{\partial t} + \check{U}_1 \frac{\partial \check{N}}{\partial x} + \check{U}_2 \frac{\partial \check{N}}{\partial y} \right) = \gamma^* \frac{\partial^2 \check{N}}{\partial y^2} - \kappa \left(2\check{N} + \frac{\partial \check{U}_1}{\partial y} \right) \tag{4}$$

$$\frac{\partial \check{T}}{\partial t} + \check{U}_1 \frac{\partial \check{T}}{\partial x} + \check{U}_2 \frac{\partial \check{T}}{\partial y} = \frac{k_{thnf}}{(\rho C_p)_{thnf}} \frac{\partial^2 \check{T}}{\partial y^2} - \frac{1}{(\rho C_p)_{thnf}} \frac{\partial \check{q}_r}{\partial y} + \frac{Q_0}{(\rho C_p)_{thnf}} (\check{T} - \check{T}_\infty) \tag{5}$$

The boundary conditions are:

$$t = 0: \check{U}_1 = \check{U}_2 = 0, \check{T} = \check{T}_\infty, t > 0: \check{U}_1 = \check{U}_w, \check{U}_2 = 0, \check{N} = 0, \check{T} = \check{T}_w, \text{ as } y = 0, \check{U}_1 \rightarrow 0, \check{N} \rightarrow 0, \check{T} \rightarrow \check{T}_\infty, \text{ as } y \rightarrow \infty \tag{6}$$

The radiative heat flux (\check{q}_r) is defined as:

$$\check{q}_r = -\frac{4\sigma^*}{3k^*} \frac{\partial \check{T}^4}{\partial y} \tag{7}$$

To linearize \check{T}^4 , we expand to:

$$\check{T}^4 \approx 4\check{T}_\infty^3 \check{T} - 3\check{T}_\infty^4 \Rightarrow \frac{\partial \check{T}^4}{\partial y} \approx 4\check{T}_\infty^3 \frac{\partial \check{T}}{\partial y} \tag{8}$$

So:

$$\frac{\partial \check{q}_r}{\partial y} = -\frac{16\sigma^* \check{T}_\infty^3}{3k^*} \frac{\partial^2 \check{T}}{\partial y^2} \tag{9}$$

Now, replace the radiation term in the energy equation:

$$\frac{\partial \check{T}}{\partial t} + \check{U}_1 \frac{\partial \check{T}}{\partial x} + \check{U}_2 \frac{\partial \check{T}}{\partial y} = \left(\frac{k_{thnf}}{(\rho C_p)_{thnf}} + \frac{16\sigma^* \check{T}_\infty^3}{3k^* (\rho C_p)_{thnf}} \right) \frac{\partial^2 \check{T}}{\partial y^2} + \frac{Q_0}{(\rho C_p)_{thnf}} (\check{T} - \check{T}_\infty) \tag{10}$$

Table 1 presents all the symbols used along with their corresponding physical meanings. The thermophysical properties of glycerine, carbon nanotubes (CNTs), gold (Au), and aluminum oxide (Al₂O₃) is displayed in Table 2.

The physical attributes of a ternary hybrid nanofluid (THN) are outlined as:

$$\phi_1 = \phi_{CNT}, \phi_2 = \phi_{Au}, \phi_3 = \phi_{Al_2O_3}$$

$$\mu_{thnf} = \frac{\mu_f}{(1 - \phi_{CNT} - \phi_{Au} - \phi_{Al_2O_3})^{2.5}}$$

$$\rho_{thnf} = (1 - \phi_{CNT} - \phi_{Au} - \phi_{Al_2O_3})\rho_f + \phi_{CNT}\rho_{s1} + \phi_{Au}\rho_{s2} + \phi_{Al_2O_3}\rho_{s3},$$

$$(\rho C_p)_{thnf} = (1 - \phi_{CNT} - \phi_{Au} - \phi_{Al_2O_3})(\rho C_p)_f + \phi_{CNT}(\rho C_p)_{s1} + \phi_{Au}(\rho C_p)_{s2} + \phi_{Al_2O_3}(\rho C_p)_{s3},$$

$$(\rho\beta)_{thnf} = (1 - \phi_{CNT} - \phi_{Au} - \phi_{Al_2O_3})(\rho\beta)_f + \phi_{CNT}(\rho\beta)_{s1} + \phi_{Au}(\rho\beta)_{s2} + \phi_{Al_2O_3}(\rho\beta)_{s3}$$

$$\sigma_{thnf} = \left[\frac{\sigma_{s1} + 2\sigma_{hnf} - 2\phi_{CNT}(\sigma_{hnf} - \sigma_{s1})}{\sigma_{s1} + 2\sigma_{hnf} + \phi_{CNT}(\sigma_{hnf} - \sigma_{s1})} \right] \sigma_{hnf},$$

$$\sigma_{hnf} = \left[\frac{\sigma_{s2} + 2\sigma_{nf} - 2\phi_{Au}(\sigma_{nf} - \sigma_{s2})}{\sigma_{s2} + 2\sigma_{nf} + \phi_{Au}(\sigma_{nf} - \sigma_{s2})} \right] \sigma_{nf}$$

$$\sigma_{nf} = \left[\frac{\sigma_{s3} + 2\sigma_f - 2\phi_{Al_2O_3}(\sigma_f - \sigma_{s3})}{\sigma_{s3} + 2\sigma_f + \phi_{Al_2O_3}(\sigma_f - \sigma_{s3})} \right] \sigma_f$$

$$k_{thnf} = \left[\frac{k_{s2} + 2k_{nf} - 2\phi_{CNT}(k_{nf} - k_{s2})}{k_{s2} + 2k_{nf} + \phi_{CNT}(k_{nf} - k_{s2})} \right] k_{hnf},$$

$$k_{hnf} = \left[\frac{k_{s1} + 2k_{hnf} - 2\phi_{Au}(k_{hnf} - k_{s1})}{k_{s1} + 2k_{hnf} + \phi_{Au}(k_{hnf} - k_{s1})} \right] k_{nf},$$

$$k_{nf} = \left[\frac{k_{s3} + 2k_f - 2\phi_{CeO_2}(k_f - k_{s3})}{k_{s3} + 2k_f + \phi_{CeO_2}(k_f - k_{s3})} \right] k_f$$

The relevant similarity variables are subsequently introduced to simplify the proposed model [12; 21].

$$\vartheta = \sqrt{\frac{by^2}{v}}, \psi = \sqrt{bv}xp(\tau, \vartheta), \check{N} = \sqrt{\frac{b}{v}}q(\tau, \vartheta), \tau = b\omega, \xi(\tau, \vartheta) = \frac{\check{T} - \check{T}_\infty}{\check{T}_w - \check{T}_\infty} \tag{11}$$

By substituting Equation 11 into Equations 3, 4 and Equation 10, we obtain the following ordinary (similarity) differential equations as follows:

TABLE 2 Thermophysical properties of glycerine, carbon nanotubes (CNTs), gold (Au), and aluminum oxide (Al₂O₃).

Thermophysical attributes	ρ (kg/m ³)	C_p (J/kg · K)	k (W/m-K)	σ (S/m)	β (K ⁻¹)
Glycerine	1260	2400	0.29	1×10^{-4}	4.82×10^{-4}
CNT	1600	425	3000	1×10^5 to 1×10^6	1.4×10^{-5}
Au	19300	129	318	4.1×10^7	1.29×10^{-5}
Al ₂ O ₃	3970	765	30	1×10^{-8}	8.5×10^{-6}

TABLE 3 Dimensionless parameters and their definitions.

Symbol	Expression	Meaning/Definition
$\Omega = \frac{\omega}{b}$	Dimensionalize frequency	Ratio of oscillation frequency ω to the characteristic strain rate b
$M = \frac{\sigma B_0^2}{b \rho_f}$	Magnetic field	Represents the strength of the applied magnetic field relative to inertial forces
$K = \frac{\kappa}{\mu_f}$	Material parameter	Indicating flow resistance in porous media
$Q_s = \frac{Q_0}{b \rho_f C_p}$	heat source /sink,	Quantifies volumetric heat generation or absorption relative to convective transport
$Pr = \frac{\nu}{\alpha}$	Prandtl number	The Prandtl number, which is the ratio of momentum to thermal diffusivity, signifies how the velocity boundary layer thickness compares to that of the thermal boundary layer
$\lambda = \frac{g_0 \beta (\bar{T}_w - \bar{T}_\infty) \chi^2 / \nu^2}{(u_w \chi / \nu)^2}$	Thermal buoyancy Parameters	Measures buoyancy force due to thermal gradients
$Rd = \frac{4 \sigma^* \bar{T}_w^3}{k_f}$	Solar radiation parameter	Indicates how dominant thermal radiation is relative to heat conduction in the overall heat transfer process
$\beta_1 = \frac{\mu_{hnf}}{\mu_f}, \beta_2 = \frac{(\rho\beta)_{hnf}}{(\rho\beta)_f}, \beta_3 = \frac{\sigma_{hnf}}{\sigma_f}, \beta_4 = \frac{k_{hnf}}{k_f},$ $\beta_5 = \frac{(\rho C_p)_{hnf}}{(\rho C_p)_f}$	Nanoparticle volume fraction	

$$\left(\frac{1}{\beta_1} + K\right)p''' + \beta_2 p p'' - \beta_2 p'^2 - (M + \delta)p' + \beta_3 \lambda \xi(1 + a \cos \pi \tau)$$

$$\cos \gamma + Kq' = \beta_2 \Omega \frac{\partial p'}{\partial \tau}, \tag{12}$$

$$\left(\frac{1}{\beta_1} + K\right)q'' - \beta_2 q' q + \beta_2 p q' - K(2q + p'') = \beta_2 \Omega \frac{\partial q}{\partial \tau}, \tag{13}$$

$$(\beta_4 + Rd)\xi'' + Pr \beta_5 p \xi' - Pr \beta_5 p' \xi = Q_s Pr \beta_5 \Omega \frac{\partial \xi}{\partial \tau}, \tag{14}$$

With

$$\left. \begin{aligned} p(\tau, 0) = q(\tau, 0) = 0, p'(\tau, 0) = 1, \xi(\tau, 0) = 1, \text{ at } \vartheta = 0 \\ p'(\tau, \vartheta) \rightarrow 0, q(\tau, \vartheta) \rightarrow 0, \xi(\tau, \vartheta) \rightarrow 0, \text{ as } \vartheta \rightarrow \infty \end{aligned} \right\} \tag{15}$$

Table 3 show the dimensionless parameters along with their symbol, expression and physical interpretations.

3 Shear drag coefficient and local Nusselt number

The Wall shear stress coefficient and the surface heat transfer coefficient are significant parameters characterizing the shear stress and thermal transport at the surface. These quantities are defined as follows:

$$Nu = \frac{xq_w}{k_f(\bar{T}_w - \bar{T}_\infty)} \tag{16}$$

And

$$C_f = \frac{2\tau_w}{\rho_f u_w^2} \tag{17}$$

where τ_w denotes the wall shear stress, and q_w represents the surface heat flux. Mathematically, it is demarcated as:

$$\tau_w = \left((\mu_{thnf} + \kappa) \frac{\partial \check{U}_1}{\partial y} + \kappa N \right)_{y=0} \tag{18}$$

the surface heat flux is defined as

$$q_w = - \left(k_{thnf} + \frac{16\sigma^* \check{T}_\infty^3}{3k^*} \right) \left(\frac{\partial \check{T}}{\partial y} \right)_{y=0} \tag{19}$$

Considering the similarity transformations mentioned above, dimensionless forms of skin friction coefficient and the Nusselt number can be obtained as follows:

$$Cf_x R_x^{1/2} = \left(\frac{1}{\beta_1 \beta_2} + K \right) p''(\tau, 0), \tag{20}$$

$$Nu_x R_x^{-1/2} = -(\beta_4 + Rd)\xi'(\tau, 0) \tag{21}$$

4 Numerical solution

Finite element method (FEM) is a method of solving a non-trivial problem that can be represented by partial differential equation. It operates by breaking the domain into small units known as elements and approximating the solution to the domain using simple functions over the element. This technique consists of discretizing, creating the equations, building a global system, prescribing the boundary conditions, and solving the unknowns. The wide applicability of FEM is based on its ability to solve complex geometries and the multi-engineering problem. To obtain solutions for Equations 12–14 together with the boundary conditions described in (15), we initially made the assumption:

$$p' = Y \tag{22}$$

The set of Equations 12–15 was transformed into a system of lower order equations.

$$\left(K + \frac{1}{\beta_1} \right) Y'' + \beta_2 p Y' - \beta_2 Y^2 - MY + \beta_3 \lambda \xi (1 + a \cos \pi \tau) \cos \gamma + Kq' - \beta_2 \Omega \frac{\partial Y}{\partial \tau}, \tag{23}$$

$$\left(\frac{1}{\beta_1} + \frac{K}{2} \right) q'' + \beta_2 p q' - \beta_2 Y q - K(2q + Y') - \beta_2 \Omega \frac{\partial q}{\partial \tau}, \tag{24}$$

$$\beta_4 \xi'' + Pr \beta_5 p \xi' - Pr \beta_5 Y \xi + Q_5 Pr \xi - Pr \beta_5 \Omega \frac{\partial \xi}{\partial \tau}, \tag{25}$$

With

$$\left. \begin{aligned} p(\tau, \vartheta) = 0, Y(\tau, \vartheta) = 1, q(\tau, \vartheta) = 0, \xi(\tau, \vartheta) = 1, \text{ at } \vartheta = 0 \\ Y(\tau, \vartheta) \rightarrow 0, q(\tau, \vartheta) \rightarrow 0, \xi(\tau, \vartheta) \rightarrow 0, \text{ as } \vartheta \rightarrow \infty \end{aligned} \right\} \tag{26}$$

For numerical computation, the plate length and thickness of boundary fixed at $\tau = 2$ and $\vartheta = 5$, respectively. The associated variational form of Equations 22–25 is given by

$$\int_{\zeta_e^*} \omega_1 \{p' - Y\} d\Omega_e^* = 0, \tag{27}$$

$$\int_{\zeta_e^*} \omega_2 \left\{ \left(\frac{1}{\beta_1} + K \right) Y'' + \beta_2 F Y' - \beta_2 Y^2 - MY + \beta_3 \lambda \xi (1 + a \cos \pi \tau) \cos \gamma + Kq' - \beta_2 \Omega \frac{\partial Y}{\partial \tau} \right\} d\Omega_e^* = 0, \tag{28}$$

$$\int_{\zeta_e^*} \omega_3 \left\{ \left(\frac{1}{\beta_1} + K \right) q'' + \beta_2 p q' - \beta_2 Y q - K(2q + \zeta') - \beta_2 \Omega \frac{\partial q}{\partial \tau} \right\} d\Omega_e^* = 0, \tag{29}$$

$$\int_{\zeta_e^*} \omega_4 \left\{ (\beta_4 + Rd)\xi'' + Pr \beta_5 p \xi' - Pr \beta_5 Y \xi + Q_5 Pr \xi - Pr \beta_5 \Omega \frac{\partial \xi}{\partial \tau} \right\} d\Omega_e^* = 0, \tag{30}$$

Here $\omega_1, \omega_2, \omega_3, \omega_4$ are arbitrary weight functions. Let divide the domain (ζ_e^*) into 4-nodded elements. The associate approximations of finite element are:

$$p = \sum_{m=1}^4 p_m \mathcal{H}_m(\tau, \vartheta), Y = \sum_{m=1}^4 Y_m \mathcal{H}_m(\tau, \vartheta), \xi = \sum_{m=1}^4 \xi_m \mathcal{H}_m(\tau, \vartheta) \tag{31}$$

here, $\mathcal{H}_m (m = 1, 2, 3, 4)$ are the linear interpolation functions for a rectangular element ζ_e and are given by

$$\begin{aligned} \mathcal{H}_1 &= \frac{(\tau_{e+1} - \tau)(\vartheta_{e+1} - \vartheta)}{(\tau_{e+1} - \tau_e)(\vartheta_{e+1} - \vartheta_e)}, \mathcal{H}_2 = \frac{(\tau - \tau_e)(\vartheta_{e+1} - \vartheta)}{(\tau_{e+1} - \tau_e)(\vartheta_{e+1} - \vartheta_e)} \\ \mathcal{H}_3 &= \frac{(\tau - \tau_e)(\vartheta - \vartheta_e)}{(\tau_{e+1} - \tau_e)(\vartheta_{e+1} - \vartheta_e)}, \mathcal{H}_4 = \frac{(\tau_{e+1} - \tau)(\vartheta - \vartheta_e)}{(\tau_{e+1} - \tau_e)(\vartheta_{e+1} - \vartheta_e)} \end{aligned} \tag{32}$$

The model of finite elements of the equations thus developed is given by:

$$\begin{bmatrix} [\mathcal{L}^{11}] & [\mathcal{L}^{12}] & [\mathcal{L}^{13}] & [\mathcal{L}^{14}] \\ [\mathcal{L}^{21}] & [\mathcal{L}^{22}] & [\mathcal{L}^{23}] & [\mathcal{L}^{24}] \\ [\mathcal{L}^{31}] & [\mathcal{L}^{32}] & [\mathcal{L}^{33}] & [\mathcal{L}^{34}] \\ [\mathcal{L}^{41}] & [\mathcal{L}^{42}] & [\mathcal{L}^{43}] & [\mathcal{L}^{44}] \end{bmatrix} \begin{bmatrix} \{p\} \\ \{Y\} \\ \{q\} \\ \{\xi\} \end{bmatrix} = \begin{bmatrix} \{\mathfrak{R}_1\} \\ \{\mathfrak{R}_2\} \\ \{\mathfrak{R}_3\} \\ \{\mathfrak{R}_4\} \end{bmatrix} \tag{33}$$

Where $[\mathcal{L}_i]$ and $[\mathfrak{R}_j] (i, j = 1, 2, 3, 4)$ are defined as:

$$\mathcal{L}_{nm}^{11} = \int_{\zeta_e} \zeta_m \frac{d\zeta_n}{d\eta} d\zeta_e \tag{34}$$

$$\mathcal{L}_{nm}^{12} = - \int_{\zeta_e} \mathcal{H}_n \mathcal{H}_m d\zeta_e^*, \mathcal{L}_{nm}^{13} = \mathcal{L}_{nm}^{14} = \mathcal{L}_{nm}^{21} = \mathcal{L}_{nm}^{31} = 0 \tag{35}$$

$$\begin{aligned} \mathcal{L}_{nm}^{22} &= - \left(\frac{1}{\beta_1 \beta_2} + K \right) \int_{\zeta_e} \frac{d\mathcal{H}_n}{d\zeta} \frac{d\mathcal{H}_m}{d\zeta} d\zeta_e^* + \int_{\zeta_e} \bar{p} \mathcal{H}_n \frac{d\mathcal{H}_m}{d\zeta} d\zeta_e^* \\ &\quad - \int_{\zeta_e} \bar{Y} \mathcal{H}_n \mathcal{H}_m d\zeta_e^* - \frac{M}{\chi_2} \int_{\zeta_e} \mathcal{H}_n \mathcal{H}_m d\zeta_e^* - \Omega \int_{\zeta_e} \mathcal{H}_m \frac{d\mathcal{H}_n}{d\tau} d\zeta_e^* \end{aligned} \tag{36}$$

$$\mathcal{L}_{nm}^{23} = \frac{K}{\chi_2} \int_{\zeta_e} \mathcal{H}_n \frac{d\mathcal{H}_m}{d\zeta} d\zeta_e^* \tag{37}$$

$$\mathcal{L}_{nm}^{24} = \frac{\chi_3 \lambda}{\chi_2} (1 + a \cos \pi \tau) \cos \gamma \int_{\zeta_e} \mathcal{H}_n \mathcal{H}_m d\zeta_e^* \tag{38}$$

$$\begin{aligned} \mathcal{L}_{nm}^{32} &= - \left(\frac{1}{\chi_1 \chi_2} + \frac{K}{2} \right) \int_{\zeta_e} \frac{d\mathcal{H}_n}{d\zeta} \frac{d\mathcal{H}_m}{d\zeta} d\zeta_e^* + \int_{\zeta_e} \bar{f} \mathcal{H}_n \frac{d\mathcal{H}_m}{d\zeta} d\zeta_e^* \\ &\quad - \int_{\zeta_e} \bar{\zeta} \mathcal{H}_n \mathcal{H}_m d\zeta_e^* - \frac{2K}{\chi_2} \int_{\zeta_e} \mathcal{H}_n \mathcal{H}_m d\zeta_e^* - \Omega \int_{\zeta_e} \mathcal{H}_n \frac{d\mathcal{H}_m}{d\tau} d\zeta_e^* \end{aligned} \tag{39}$$

TABLE 4 Convergence, grid independence, and computational performance.

Grid size	Iterations to converge	Max residual at convergence	Skin friction coefficient (C_f)	Nusselt number (Nu_x)	CPU time per iteration (s)
21 × 21	173	9.8×10^{-7}	0.2810	3.505	0.010
31 × 31	179	8.4×10^{-7}	0.2856	3.540	0.016
41 × 41	185	7.2×10^{-7}	0.2874	3.568	0.021
61 × 61	192	6.3×10^{-7}	0.2901	3.591	0.039
81 × 81	198	5.9×10^{-7}	0.2909	3.597	0.062
101 × 101	203	5.4×10^{-7}	0.2913	3.600	0.095
121 × 121	208	4.9×10^{-7}	0.2916	3.603	0.138
141 × 141	213	4.5×10^{-7}	0.2916	3.603	0.184

TABLE 5 Numerical outcomes of the Nusselt number for the distinct values of the Prandtl number.

Pr	Present outcomes	[31]	[32]
0.72	-0.808633	-0.8086	-0.8088
1.00	-0.808633	-0.8086	-0.8088
3.00	-0.808633	-0.8086	-0.8088
10.0	-0.808633	-0.8086	-0.8088

$$\mathcal{L}_{nm}^{33} = -\frac{K}{\chi_2} \zeta_n \frac{d\mathcal{H}_m}{d\zeta} d\zeta_e^* \tag{40}$$

$$\mathcal{L}_{nm}^{34} = \mathcal{L}_{nm}^{33} = \mathcal{L}_{nm}^{42} = \mathcal{L}_{nm}^{43} = 0 \tag{41}$$

$$\begin{aligned} \mathcal{L}_{nm}^{44} = & -\frac{\beta_4}{\beta_5} \int_{\zeta_e^*} \frac{d\mathcal{H}_n}{d\zeta} \frac{d\mathcal{H}_m}{d\zeta} d\zeta_e^* + \text{Pr} \int_{\zeta_e^*} \bar{p} \mathcal{H}_n \frac{d\mathcal{H}_m}{d\zeta} d\zeta_e^* \\ & - \text{Pr} \int_{\zeta_e^*} \bar{\xi} \mathcal{H}_n \mathcal{H}_m d\zeta_e^* - \text{Pr} \Omega \int_{\zeta_e^*} \mathcal{H}_n \frac{d\mathcal{H}_m}{d\xi} d\zeta_e^* \\ & + \text{Pr} \frac{Q_s}{\chi_5} \int_{\zeta_e^*} \bar{\xi} \mathcal{H}_n \mathcal{H}_m d\zeta_e^* \end{aligned} \tag{42}$$

Figure 1B shows the step-by-step procedure involved in the Finite Element Method (FEM). The process starts with defining the physical problem, followed by discretization of the domain into finite elements. Element equations are formulated using shape functions and assembled into a global system. Table 4 shows convergence characteristics, skin friction coefficient, Nusselt number and number of computational times per iteration using various grid sizes applied in finite difference method. The aim of the study is to provide a grid-independent and computationally efficient numerical solution. The comparison of the considered code for the limiting cases are presented in Table 5. The numerical results show strong agreement with previously published data, confirming the reliability and precision of the computational model.

5 Results and discussion

The numerical simulations provided detailed insight into how gravitational modulation, magnetic field strength, and

nanoparticle composition influence both flow dynamics and thermal behavior of micropolar nanofluids over the inclined stretching sheet. Figure 2 reveals how the $Nu_x R_x^{-1/2}$ varies as the material parameter (k) upsurges for three kind of nanofluids: traditional nanofluids, CNT- Au-Al₂O₃/Glycerine ternary hybrid nanofluids and CNT-Au\Glycerine hybrid nanofluids. The horizontal axis signifies the material parameter over the interval from 0 to 3, while the vertical axis shows the $Nu_x R_x^{-1/2}$, which describes the thermal transport rate. With increasing values of material parameter (k), $Nu_x R_x^{-1/2}$ is also enlarged in all kinds of nanofluids, displaying that an increase in material parameter results in an increase in convective heat transfer. The $Nu_x R_x^{-1/2}$ of CNT- Au-Al₂O₃/Glycerine ternary hybrid nanofluids is also found to be the greatest, out of all the three curves. The CNT- Au\Glycerine hybrid nanofluids are intermediate between CNT- Au-Al₂O₃/Glycerine ternary hybrid nanofluids and the traditional nanofluids whereby it can outperform the traditional nanofluids but cannot do so well as the ternary hybrids.

The $p'(\tau, \vartheta)$ within the momentum boundary layer is significantly affected via the M parameter, as showed in Figure 3A. As value of the Magnetic field parameter improved, the $p'(\tau, \vartheta)$ reduce. This decrease in velocity is caused by the Lorentz force generated through the applied transverse magnetic field, a resistive dragging force on the flowing electrically conducting nanofluid. Basically, the magnetic field presents an additional body force opposing the velocity direction, thereby obstructing momentum transmission and slowing the velocity field. An increase in the magnetic field parameter significantly reduces the velocity profile by strengthening the opposing Lorentz force, which suppresses fluid motion and stabilizes the flow, and this mechanism is widely applied in controlling electrically conducting fluids in metallurgical processing, MHD power generation, nuclear reactor cooling, biomedical flow control, and microfluidic devices. The physical interpretation of such a phenomenon can be the conversion of kinetic energy to the dissipation of magnetic energy. The greater the field applied (the larger M), the larger the deceleration, and thinner the momentum boundary layer. The viscous shear stress increases because the increase at the velocity gradient is high at the wall.

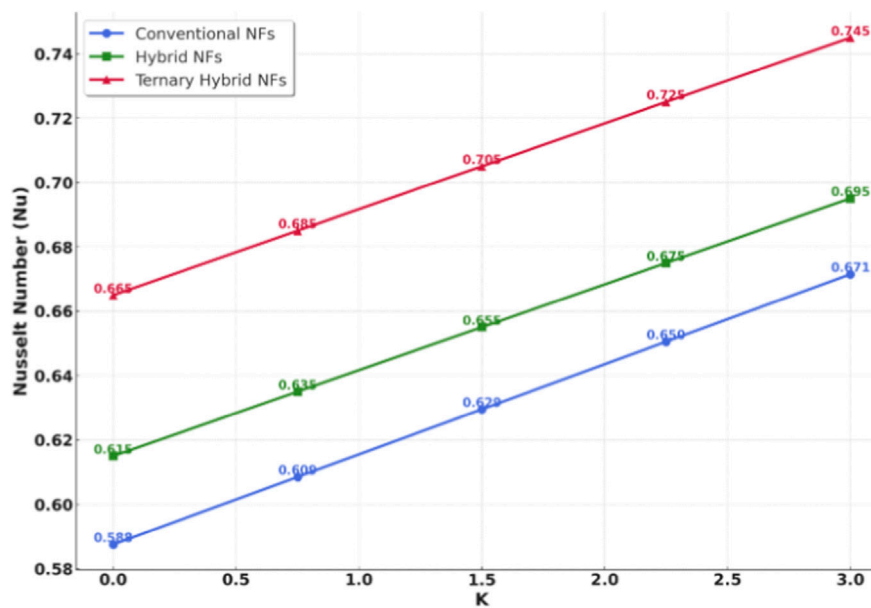


FIGURE 2
Graphical illustration of the thermal transport rate versus M .

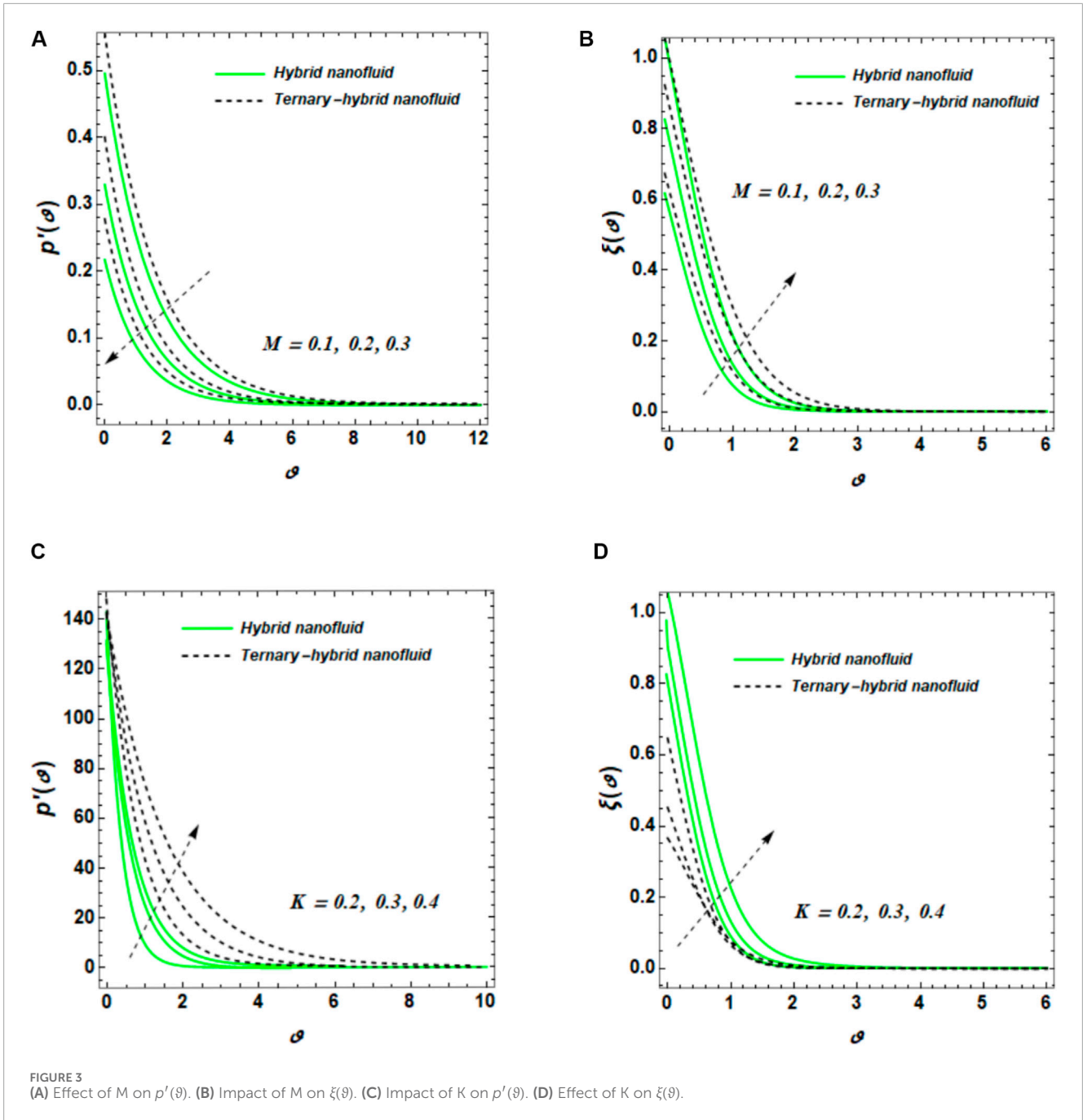
The M parameter displays the important effect on the $\xi(\tau, \vartheta)$ temperature profile within the boundary layer of the CNT-Au-Al₂O₃/glycerine based fluid, as revealed in Figure 3B. As M parameter upsurges, the $\xi(\tau, \vartheta)$ increase consistently across fluid system. This performance stems from the relations between the applied transverse magnetic and the conducting ternary hybrid nanofluid. In practical applications, the occurrence of the magnetic field produces a Lorentz force performing opposite to the path of the flow behavior, effectively slowing the liquid particles. When the $\xi(\tau, \vartheta)$ reduces as result of magnetic damping, the convective motion of heat away from the surface reduces, leading to a thicker thermal boundary layer and higher $\xi(\tau, \vartheta)$. This greater retention of thermal energy shows as greater $\xi(\tau, \vartheta)$. Physically, the magnetic field reduces kinetic energy, thereby growing the thermal energy retained near the heated surface. The CNT-Au-Al₂O₃/glycerine based fluid further increase this occurrence since their great thermal conductivity facilitates faster thermal transport from the wall into the fluid, system but the slowed flow behavior limits the dissipation of this heat.

The micropolar material parameter K drastically impact the $p'(\tau, \vartheta)$ in the boundary layer, as exhibited in Figure 3C. As value of micropolar material parameter upsurges, the $p'(\tau, \vartheta)$ show an improvement. This is a direct consequence of micropolar fluid characteristics, which allow for micro-rotation of fluid particles and couple stress effects absent in Newtonian fluids. This can be attributed directly to the nature of micropolar fluids, which enable micro-sliding of fluid particles and couple stress, which are not possible in Newtonian fluids. Physically, an increase in K means that the material has a greater microrotational viscosity or spin-translational coupling of the microelements and the fluid translation. This increased coupling lowers the effective viscosity against the flow and allows faster flow closer to the wall. Furthermore, the spin inertia can also enhance a slip-like interaction

at the interface, lowering the friction and further increasing the velocity distribution. This performance has significant relevance in engineering systems employing micropolar or microstructured liquids, such as lubricants comprising microspheres, fluid crystals, or blood flow in microchannels. In microfluidic devices, greater K can increase flow rates and mixing, which is required for applications such as microfluidic chips and medical laboratory science.

The influence of the K parameter on $\xi(\tau, \vartheta)$ is important, as observed in Figure 3D. As K upsurges, the $\xi(\tau, \vartheta)$ display a rise all over the thermal boundary layer. This intensification happens since the improved micro-rotation influence and coupling stresses in micropolar liquids upsurge momentum transport, which in turn affects the conservation of energy in a fluid flow via encouraging stronger conductive and convective thermal transport mechanisms close to the wall. The phenomenon has important consequences in technologies that use micropolar fluids to overcome thermal management. As the parameter of the micropolar material parameter increases, thermal distributions increase due to the stronger coupling of micro-rotation and heat transport. The effect enables the performance of enhanced heat transfer in the micropolar nanofluid systems, and is beneficial in the design of more advanced thermal control and biomedical engineering devices.

The performance of the $\xi(\tau, \vartheta)$ in response to variations in the heat source/sink parameter Q_s is demonstrated in Figures 4A,B shows the effect of positive values of ($Q_s > 0$), signifying a heat source, whereas Figure 4A signifies the influence of negative values of heat sink ($Q_s < 0$). In Figure 4A, as the value of Q_s upsurges from, the $\xi(\tau, \vartheta)$ becomes more significant throughout the thermal boundary layer region. This reveals that the occurrence of a $Q_s > 0$ enhances heat energy within the fluid, thereby growing temperature gradients. On the other hand, Figure 4B, as the value of Q_s becomes



increasingly negative, the $\xi(\tau, \theta)$ reduces more rapidly. The physical reasoning behind this action is due to the energy equation that forms the heat transport in the boundary layer. With a heat source, the production of internal thermal energy causes net heat gain, increasing conduction and convection in the medium. This automatically leads to increased fluid temperatures. Conversely, a heat sink reflects the inner energy absorption or heating exhaustion, removing the energy inside the system, thus reducing the local temperature field. Comparison of the ternary hybrid nanofluid and hybrid nanofluid Figure 4A, and Figure 4B indicate that the hybrid nanofluid preserves a higher amount of thermal energy.

The effect of the M parameter on the $Cf_x R_x^{1/2}$ is graphically shown in the Figure 4C. The result exposes that as M upsurges, there is a noticeable increase in the $Cf_x R_x^{1/2}$ for both ternary hybrid nanofluid and hybrid nanofluid. This rise in surface shear stress is actually ascribed to the additional of a Lorentz force within the electrically conducting liquid das a result of a magnetic field. The Lorentz force acts perpendicular to both the flow speed and magnetic field, creating a resistive force that acts against flow movement. Therefore, more shear is established close the surface to counterbalance this resistive influence, thereby improving the $Cf_x R_x^{1/2}$.

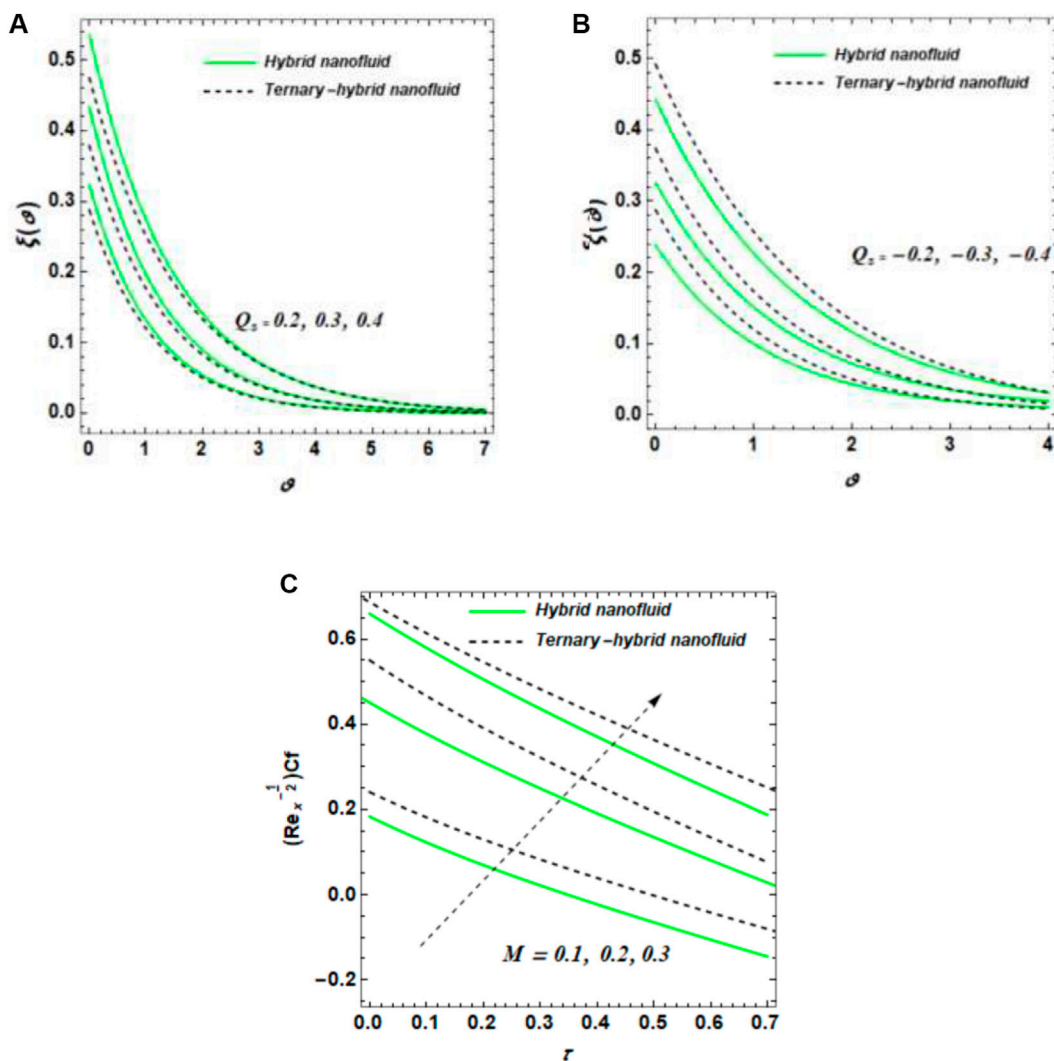


FIGURE 4 (A) Effect of ($Q_s > 0$) on $\xi(\theta)$. (B) Effect of ($Q_s < 0$) on $\xi(\theta)$. (C) Impact of M on $Cf_x R_x^{1/2}$.

The influence of the K parameter on $Cf_x R_x^{1/2}$ is shown in Figure 5A. As micropolar material parameter upsurges, the $Cf_x R_x^{1/2}$ Undergoes a corresponding enlargement for both ternary hybrid nanofluid and hybrid nanofluid. Micropolar fluids are distinct of conventional Newtonian fluids because they are characterized as possessing microstructures and being able to bear microrotation effects. The micropolar material parameter is a measure of the strength of coupling of the micro-rotational effects of the particles and the macroscopic velocity field. The larger the value of K , the more intense the coupling and the greater the rotational viscosity.

The graphical outcomes showed in Figures 5B,C demonstrate the dynamic effect of two significant parameters namely, the frequency parameter (Ω) and the inclined angle (γ) on the $Cf_x R_x^{1/2}$ and the $Nu_x R_x^{-1/2}$ in the presence of both ternary hybrid nanofluid and hybrid nanofluid,. These Figures reveal how oscillatory performance in the fluid system and orientation of the surface alter the dynamic motion and heat transfer boundary layers. From

Figure 5B, the influence of the (Ω) on the $Nu_x R_x^{-1/2}$ is seen. As Ω upsurges from 0.2 to 1.0, the amplitude of oscillations in $Nu_x R_x^{-1/2}$ increases for both ternary hybrid nanofluid and hybrid nanofluid. For increasing value of Ω , the ternary hybrid nanofluid consistently shows greater $Nu_x R_x^{-1/2}$ than the hybrid nanofluid, confirming its superior ability to transport momentum as a result of the improved effective viscosity and density brought about via the mixture of nano-sized particles. Physically, increasing skin friction as a result of increasing the frequency is related to an increase in oscillatory movement out in the boundary of the layer generating movement resistance to the movement of the fluid. This opposition is due to the inertia of the fluid particles that strive to adhere to the oscillating plate and is greater with hybrid nanofluids since their momentum diffusivity is also larger. The $Cf_x R_x^{1/2}$ is investigated against the inclined angle γ . Here, as γ increases from 0 to $\pi/3$, a remarkable increase in $Cf_x R_x^{1/2}$ is observed for both nanofluids, more prominently for the ternary hybrid nanofluid. This phenomenon can be justified by the presence of

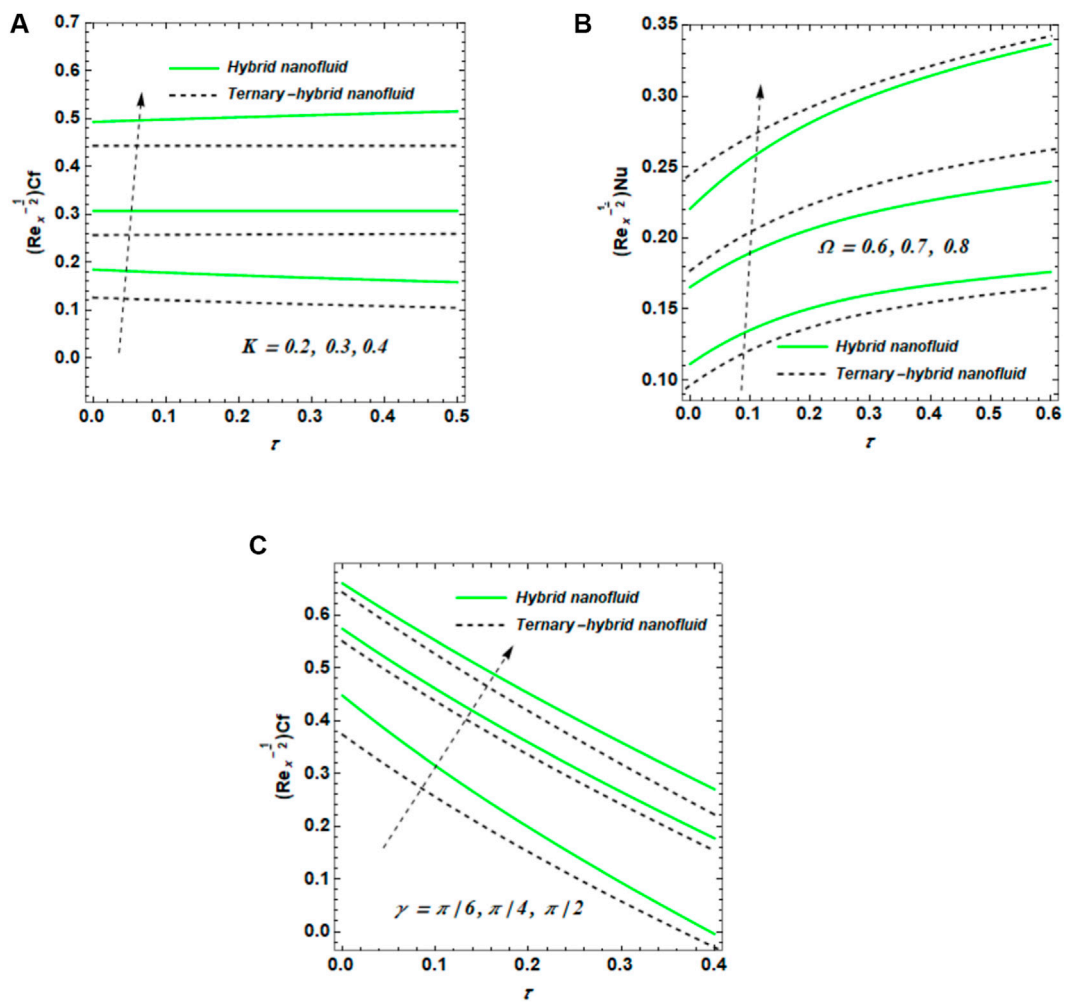


FIGURE 5 (A) Impact of K on $Cf_x R_x^{-1/2}$. (B) Impact of Ω on $Nu_x R_x^{-1/2}$. (C) Impact of γ on $Cf_x R_x^{-1/2}$.

the gravitational component that operates opposite to the inclined plane and stimulates the interaction of the layers of the fluid and makes the shear rate higher around the wall. The gravitational assist boosts the pressure drag significantly but causes increased viscous shear to increase the skin friction. Figure 5B shows the influence of the γ on the heat transfer rate a key indicator of convective heat transfer. Interestingly, the results show a slight decline in the Nusselt number as the inclined angle increases. This decreasing trend is evident for both THNFs and THNFs nanofluids, with the hybrid still maintaining a higher overall heat transfer rate. The reduction in with increasing γ can be attributed to the diminished thermal boundary layer disturbance caused by gravity, which tends to align the flow more closely with the inclined surface, reducing convective mixing in the normal direction. Essentially, convective heat extinguishing is less efficient as the surface becomes tipped, due to the decreased strength of the buoyancy forces that is contributing to the vertical heat transport.

The velocity distribution shows the decreasing pattern as the nanoparticle parameter increases, which is demonstrated in Figure 6A. The velocity distribution shows the decreasing

pattern as the nanoparticle parameter increases, which is also demonstrated in Figure 6A. The inverse relation can be explained by the fact that the introduction of the greater quantities of the nanoparticles leads to the higher effective viscosity of the nanofluid and its density. When solid particles are included in the fluid mass, the internal frictional resistance caused by the particles rises as does the measure of fluid-flow restriction. As a result, the fluid particles momentum is reduced, causing the velocity boundary layer to be thin and decreasing the total flow velocity. The added inertial drag fluid viscosity due to the suspended particles is overwhelming the driving forces due to the acceleration of the fluid hence slowing down the movement.

Figure 6B clearly reveals the important role that nanoparticle volume fraction plays in modifying the velocity and thermal fields of the fluid. As the nanoparticle volume fraction upsurges, the temperature profile dramatically improved, whereas the fluid flow reduces. The phenomenon lies in the significant change that occurs in the addition of nanoparticles to the base fluid, especially their thermophysical properties. A higher nanoparticle parameter can be physically explained by the increased thermal conductivity through

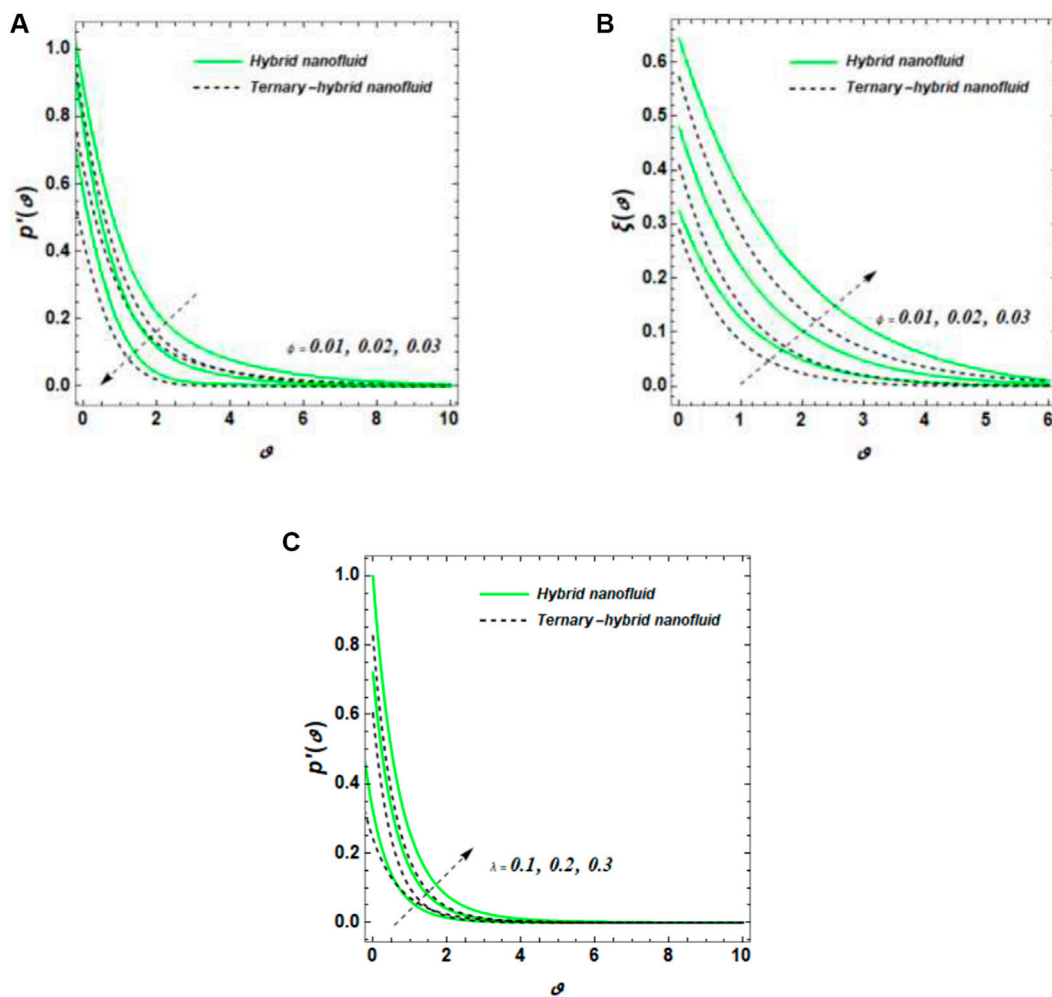


FIGURE 6

(A) Effect of nanoparticle volume fraction on $p'(\vartheta)$. (B) Effect of nanoparticle volume fraction on $\zeta(\tau, \vartheta)$. (C) Effect of thermal buoyancy parameter on $p'(\vartheta)$.

the suspended solid particles that tend to increase the thermal distribution. When these particles are well distributed in the fluid, these particles greatly enhance the heat transfer capacity of the fluid. Consequentially, the thermal boundary layer is thickened, and a general increase of the fluid temperature close to the heated surface takes place. The nanoparticles serve as a very effective heat carrier which traps the heat energy at the surface and transports it along the fluid more efficiently than through molecular conduction. This improved mechanism of heat transfer leads to increased temperature profile as seen in Figure 6B.

The impact of the thermal buoyancy parameters on the velocity field as seen in Figure 6C has a distinct implication showing a significant increase in the flow velocity as the buoyancy strength increases. Thermal buoyancy occurs when temperature gradients in a fluid cause density changes leading to buoyant forces that are directed opposite to the direction of gravity. Such forces may assist the fluid flow or resist it depending on geometry and discrepancies between fluid temperatures. In the specified example, the parameter of buoyancy has a positive impact on the fluid flow, that is, the velocity profile becomes more powerful due to its amplification.

This phenomenon is a direct result of thermo-momentum coupling where increasing temperature gradients both move heat but also result in flow by driving buoyant acceleration. Practically, the impact of thermal buoyancy is extraordinarily significant in numerous engineering applications which involve natural convection, which include solar collectors, passive electronic cooling systems, building ventilations, nuclear reactor coolants, and heat exchangers. In such systems, it is often desirable to increase buoyant flow so as to increase the natural circulation of fluids without mechanical pumps. As an example, when placed in solar thermal collectors, the use of greater thermal buoyancy will enable greater thermo-hydraulic circulation within the working fluid and, therefore, greater heat absorption and transport.

6 Conclusion

This study has numerically explored the combined effects of gravitational modulation, magnetic field intensity, internal heat generation or absorption, and advanced nanoparticle

compositions on the convective transport behavior of micropolar nanofluids over an inclined stretching sheet in a microgravity environment. By incorporating the thermophysical properties of glycerine, carbon nanotubes, gold, and aluminum oxide into the formulation of hybrid nanofluids, the analysis has demonstrated that these complex suspensions can substantially enhance both fluid velocity and thermal distribution compared to conventional mono-nanofluids.

- The outcomes reveal that the M parameter dramatically upsurges $\xi(\tau, \vartheta)$ due to the conversion of kinetic energy into heat via Lorentz forces, while it reduces fluid flow due to magnetic resistance.
- The k parameter improves $p'(\tau, \vartheta)$ as micro-rotations lower local viscosity, but it decreases $\xi(\tau, \vartheta)$ via dispersing heat more efficiently.
- The heat source/sink parameter ($Q_s > 0$, $Q_s < 0$) displays dual performance positive values (source) increase $\xi(\tau, \vartheta)$, whereas negative values (sink) decrease it.
- Moreover, both M and K parameter upsurge $Cf_x R_x^{1/2}$ due to higher boundary resistance.
- Frequency and inclined angle parameters also raise $Cf_x R_x^{1/2}$, though the inclined angle reduces the $Nu_x R_x^{-1/2}$, signifying a decline in thermal transfer rate.
- The nanoparticle parameter increases $\xi(\tau, \vartheta)$ through enhanced conductivity but decreases $p'(\tau, \vartheta)$ due to additional drag.
- Thermal buoyancy parameters improve $p'(\tau, \vartheta)$ by introducing additional driving force due to temperature-induced density differences.
- These outcomes are vital for optimizing fluid and thermal transport in energy, medical engineering, and industrial uses.

6.1 Real-life applications

The outcomes of this study offer practical value for several engineering sectors operating in reduced-gravity or space environments. The demonstrated enhancement in heat and momentum transport using ternary hybrid nanofluids can support the development of more efficient thermal control systems in satellites, spacecraft, and orbital platforms. Improved heat removal capability is particularly beneficial for regulating the temperature of onboard electronics, solar panels, propulsion units, and advanced sensors in microgravity. In aerospace engineering, the findings can be applied to high-altitude vehicles and re-entry systems where gravitational fluctuations influence boundary-layer behavior.

6.2 Potential future extensions

In future work, the present study can be extended by considering more complex nanofluid models, such as tetra-hybrid or multi-component nanofluids, and incorporating non-Newtonian behavior for more realistic applications. The effects of time-dependent or oscillating magnetic and electric fields, as well as chemical reactions, could be analyzed to better understand their

impact on flow and heat transfer. Transient and three-dimensional analyses may also be performed to investigate flow instabilities, while experimental validation can be carried out to confirm numerical results and support potential industrial applications in cooling systems, microelectronics, biomedical devices, and energy systems.

Data availability statement

The raw data supporting the conclusions of this article will be made available by the authors, without undue reservation.

Author contributions

RS: Investigation, Writing – original draft, Validation, Visualization, Data curation. SA: Validation, Writing – review and editing, Software, Funding acquisition, Writing – original draft, Project administration. AO: Methodology, Writing – original draft, Software, Conceptualization, Validation, Formal Analysis. AI: Software, Conceptualization, Formal Analysis, Writing – original draft, Validation, Methodology. UK: Supervision, Conceptualization, Resources, Writing – original draft, Writing – review and editing.

Funding

The author(s) declared that financial support was not received for this work and/or its publication.

Conflict of interest

The author(s) declared that this work was conducted in the absence of any commercial or financial relationships that could be construed as a potential conflict of interest.

Generative AI statement

The author(s) declared that generative AI was not used in the creation of this manuscript.

Any alternative text (alt text) provided alongside figures in this article has been generated by Frontiers with the support of artificial intelligence and reasonable efforts have been made to ensure accuracy, including review by the authors wherever possible. If you identify any issues, please contact us.

Publisher's note

All claims expressed in this article are solely those of the authors and do not necessarily represent those of their affiliated organizations, or those of the publisher, the editors and the reviewers. Any product that may be evaluated in this article, or claim that may be made by its manufacturer, is not guaranteed or endorsed by the publisher.

References

- Ahmed SE, Mansour MA, Mahdy A, Mohamed SS. Entropy generation due to double diffusive convective flow of Casson fluids over nonlinearity stretching sheets with slip conditions. *Eng Sci Technol Int J* (2017) 20(6):1553–62. doi:10.1016/j.jestch.2017.10.002
- Alshuhail LA, Shaik F, Sundar LS. Thermal efficiency enhancement of mono and hybrid nanofluids in solar thermal applications—A review. *Alexandria Eng J* (2023) 68:365–404. doi:10.1016/j.aej.2023.01.043
- Abbas A, Hussanan A, Anwar F, Obalalu AM, Almeshaal MA, Palaniappan M, et al. Thermal analysis of AA7075 AA7072/methanol via Williamson hybrid nanofluid model past thin needle: effects of Lorentz force and irregular heat rise/fall. *Case Stud Therm Eng* (2024) 53:103883. doi:10.1016/j.csite.2023.103883
- Shamshuddin MD, Saeed A, Asogwa KK, Usman and Jamshed W. A semi analytical approach to investigate the entropy generation in a tangent hyperbolic magnetized hybrid nanofluid flow upon a stretchable rotating disk. *J Magnetism Magn Mater* (2023) 574:170664. doi:10.1016/j.jmmm.2023.170664
- Al-Turef GA, Obalalu AM, Saleh W, Shah SHAM, Darvesh A, Khan U, et al. Computational study and application of the Hamilton and crosser model for ternary hybrid nanofluid flow past a rigid wedge with heterogeneous catalytic reaction. *Nano* (2025) 97(12):1277–87. doi:10.1142/S1793292024501054
- Bilal S, Yasir M. Mass transpiration impact on effectiveness of heat transport of ternary hybrid nanofluid with velocity slip. *Case Stud Therm Eng* (2025) 66:99–105. doi:10.1016/j.csite.2025.106530
- Khan H, Yaseen M, Rawat SK, Khan A. Insights into the significance of ternary hybrid nanofluid flow between two rotating disks in the presence of gyrotactic microorganisms. *Nano* (2025) 311:147–56. doi:10.1142/S1793292024501108
- Bhattad A, Atgur V, Rao BN, Banapurmath NR, Yunus Khan TM, Vadlamudi C, et al. Review on mono and hybrid nanofluids: preparation, properties, investigation, and applications in IC engines and heat transfer. *Energies* (2023) 16(7):3189. doi:10.3390/en16073189
- Gorla RSR, Chamkha A. Natural convective boundary layer flow over a nonisothermal vertical plate embedded in a porous medium saturated with a nanofluid. *Nanoscale Microscale Thermophysical Eng* (2011) 15(2):81–94. doi:10.1080/15567265.2010.549931
- Huminic G, Huminic A. Heat transfer capability of the hybrid nanofluids for heat transfer applications. *J Mol Liquids* (2018) 272:857–70. doi:10.1016/j.molliq.2018.10.095
- Bixapathi S, Babu AB. Analyzing the effects of internal heating and chemical reactions in a porous layer due to a vertical oblique magnetic field and gravity modulation. *Phys Fluids* (2025) 233:4551–65. doi:10.1063/5.0250097
- Jakhar A, Anurag A, Kumar A. Weakly nonlinear instability analysis in triple-diffusive convection under gravity modulation in the presence of an internal heat generator. *Heat Transfer* (2025) 54(1):167–183. doi:10.1002/htj.23087
- Isa S, Parvin S, Arifin N, Ali F, Ahmad K. Soret-Dufour effects on the water-based hybrid nanofluid flow with nanoparticles of Alumina and copper. *Malaysian J Mathematics Sci* (2023) 15(19):3419. doi:10.47836/mjms.17.3.04
- Eswaramoorthi S, Thamaraiselvi S, Loganathan K. Exploration of Darcy Forchheimer flows of Non-Newtonian Casson and Williamson conveying tiny particles experiencing binary chemical reaction and thermal radiation: comparative analysis. *Math Comput Appl* (2022) 27(3):52. doi:10.3390/mca27030052
- Arya AS, Sudharani MV, Reddy MG, Prakasha DG, Kumar KG. Stratified heat generation in magnetohydrodynamics dissipative flow micropolar fluid through curved surface: a computational analysis. *Int J Thermofluids* (2025) 13(11):3192. doi:10.1016/j.ijft.2025.101265
- Abbas S, Nazar M. Fractional analysis of unsteady magnetohydrodynamics Jeffrey flow over an infinite vertical plate in the presence of Hall current. *Math Methods Appl Sci* (2025) 48(1):253–72. doi:10.1002/mma.10326
- Dogonchi AS, Waqas M, Afshar SR, Seyyedi SM, Hashemi-Tilehnoee M, Chamkha AJ, et al. Investigation of magneto-hydrodynamic fluid squeezed between two parallel disks by considering Joule heating, thermal radiation, and adding different nanoparticles. *Int J Numer Methods Heat Fluid Flow* (2020) 30(2):659–80. doi:10.1108/hff-05-2019-0390
- Alshammari S, Ullah Z, Alam MM, Boujelbene M, Ibrahim AO, Abu-Zinadah H. Periodic and time-mean fluctuating heat transfer of Darcy nanofluid along nonlinear radiating plate with heat source/sink and oscillatory amplitude conditions. *Chaos, Solitons and Fractals* (2025) 481(1):233–43. doi:10.1016/j.chaos.2025.116229
- Hayat T, Ijaz M, Qayyum S, Ayub M, Alsaedi A. Mixed convective stagnation point flow of nanofluid with Darcy-Fochheimer relation and partial slip. *Results Phys* (2018) 9:771–8. doi:10.1016/j.rinp.2018.02.073
- Sandhya M, Ramasamy D, Sudhakar K, Kadirgama K, Harun WSW. Ultrasonication an intensifying tool for preparation of stable nanofluids and study the time influence on distinct properties of graphene nanofluids—A systematic overview. *Ultrason Sonochem* (2021) 73:105479. doi:10.1016/j.ultrsonch.2021.105479
- Shobha V, Mulki H, Baskar P, Raju SSK, Mahmoud S, Abdrabboh M, et al. Non-Linear thermal radiation analysis of electromagnetic chemically reacting ternary nanofluid flow over a bilinear stretching surface. *Results Eng* (2025) 51(6):433–43. doi:10.1016/j.rineng.2024.103841
- Gireesha BJ, Pavithra CG, Gorla RSR. Enhanced heat transfer analysis of Casson hybrid nanofluid in blood with thermal radiation through a stretching sheet: a comprehensive study of analytical and numerical method. *Proc Inst Mech Eng N: J Nanomater Nanoengineering Nanosystems* (2025) 12(4):41–54. doi:10.1177/23977914241304063
- Tabrez M, Azeem Khan W. Exploring physical aspects of viscous dissipation and magnetic dipole for ferromagnetic polymer nanofluid flow. *Waves in Random and Complex Media* (2022) 35:1–20. doi:10.1080/17455030.2022.2135794
- Sreenivasulu P, Bilal S, Poornima T. Thermal performance of a micropolar fluid flowing around a vertical cone with consideration of spatially varying heat source. *Case Stud Therm Eng* (2025) 333:4342–131. doi:10.1016/j.csite.2024.105576
- Asghar Z, Khan MWS, Ali N, Waqas M. On IFDM simulation of Oldroyd 8-constant fluid flowing due to motile microorganisms. *Chin J Phys* (2025) 93:158–71. doi:10.1016/j.cjph.2024.11.033
- Asghar Z. Surface roughness effects on the propelling mechanism of spermatozoa. *The Eur Phys J Plus* (2024) 139(10):876. doi:10.1140/epjp/s13360-024-05686-y
- Asghar Z, Khan MWS, Gondal MA, Ghaffari A. Magnetohydrodynamic flow of Carreau Yasuda fluid inside a complex wavy passage formed by beating cilia: a finite-difference analysis. *Proc Inst Mech Eng E: J Process Mech Eng* (2025) 239(1):87–98. doi:10.1177/09544089231171037
- Asghar Z, Shah RA, Ali N. A numerical framework for modeling the dynamics of micro-organism movement on Carreau-Yasuda layer. *Soft Comput* (2023) 27(13):8525–39. doi:10.1007/s00500-023-08236-3
- Asghar Z, Khan MWS, Shatanawi W, Gondal MA, Ghaffari A. An IFDM analysis of low Reynolds number flow generated in a complex wavy curved passage formed by artificial beating cilia. *Int J Mod Phys B* (2023) 37(19):2350187. doi:10.1142/s0217979223501874
- Dogonchi AS, Asghar Z, Waqas M. CVFEM simulation for Fe₃O₄-H₂O nanofluid in an annulus between two triangular enclosures subjected to magnetic field and thermal radiation. *Int Commun Heat Mass Transfer* (2020) 112:104449. doi:10.1016/j.icheatmasstransfer.2019.104449
- Sharidan S, Amin N, Pop I. G-jitter mixed convection adjacent to a vertical stretching sheet. *Microgravity-Science Technology* (2023) 18:4313–9. doi:10.1007/bf02908414
- Ali B, Khan SA, Hussein AK, Thumma T, Hussain S. Hybrid nanofluids: significance of gravity modulation, heat source/sink, and magnetohydrodynamic on micropolar fluid over an inclined surface via finite element simulation. *Appl Mathematics* (2022) 27(15):143–56. doi:10.1016/j.amc.2021.126878